Hydrodynamics, heat transfer and kinetics reaction of CFD modeling of a batch stirred reactor under hydrothermal carbonization conditions

Diakaridia Sangare, Stéphane Bostyn, Mario Moscosa-Santillan, Iskender Gökalp

Hydrodynamics, heat transfer and kinetics reaction of CFD modeling of a batch stirred reactor under hydrothermal carbonization conditions

Diakaridia Sangare[1,2], Stéphane Bostyn[2,3,*], Mario Moscosa-Santillan[1], Iskender Gökalp[2]

[1] Facultad de Ciencias Químicas Universidad Autónoma de San Luis Potosí Av. Dr. Nava # 6, Zona Universitaria San Luis Potosí, S.L.P., CP: 78210, México

[2] Institut de Combustion, Aérothermique, Réactivité, et Environnement (ICARE)-CNRS UPR3021, 1C avenue de la recherche scientifique 45071 Orléans Cedex 2, France

[3] Université d'Orléans, Institut Universitaire de Technologie, 16 rue d'Issoudun BP16724 45067 Orléans Cedex 2, France

* Correspondence: Email: stephane.bostyn@univ-orleans.fr; Tel: +33238255476; Fax: +33238696004.

Abstract: Computational Fluid Dynamics simulation was used to study hydrothermal carbonization of avocado stone (AS) in a batch stirred reactor, using an open-loop controller system. The corresponding simulations were carried out in COMSOL Multiphysics 5.2. The different biomass-to-water ratio was investigated. The hydrodynamic study shows that the ideal stirring speed to obtain a homogeneous mixture inside the reactor is 550 rpm, due to the high density of AS particles (1547.64±27.33 kg/m^3). However, a stagnant zone was observed just below the impeller. To validate the CFD simulations temperature profiles with experimental data, the heat transfer coefficient of the insulator was determined (11.66 W/m^2.K), this value was used to set the heat loss in the CFD simulation. According to the model, the difference between the thermal properties of biomass and water under hydrothermal carbonization conditions is negligible. However, experimentally, an increase in temperature was observed with increasing biomass to-water-ratio; this is due to the global hydrothermal carbonization of AS is exothermic reaction. The heat released during 8 hours, including heat-up time, was -7.25 ±0.32MJ/kg of feedstock. Finally, a kinetic model was proposed taking into account the influence of temperature, heat-up time, reactor volume, and biomass concentration.

Keywords: Avocado Stone; Hydrothermal Carbonization; CFD Modeling, Stirred Reactor, Open-Loop Controller system, Hydrodynamics, Heat Transfer, Kinetic Model.

1 INTRODUCTION

The production of clean and sustainable fuels is the main challenge of the upcoming energy crisis and climate change. The potential of lignocellulosic biomass as an abundant source of renewable energy. Although there are different processes to convert biomass into energy, its direct use as fuel, faces several challenges (inefficiency of conversion facility, low-energy, biological instability, high moisture content, and so forth [1]. Pretreatment processes are necessary to improve the organic feedstock characteristics for most biomass to energy conversion processes.

Hydrothermal carbonization (HTC), also known as a wet thermochemical process, emulates the natural process of coalification, virtually no pretreatment is required [2]. HTC is a thermochemical conversion process by which biomass is converted into carbonized material (hydrochar), liquid (bio-oil mixed with water) and small fractions of gases; this process is performed in the temperature range of 180-250°C under autogenous saturated vapor pressure between 10 and 40 bars, and a residence time range from a few minutes up to several hours [3-5]. The performance and composition of the final products are directly related to biomass type, and process conditions such as reaction temperature, residence time, and water-to-biomass ratio. HTC process has investigated distinct types of biomass; sugarcane bagasse [6], corn cob [7], tomato waste [8], olive pomace [4], olive stones [9], and so forth. Most of these biomasses are agro-industrial wastes, in Mexico, one of the most significant agro-industrial wastes generated is avocado stones (AS). The products of HTC can be used directly as a solid fuel, soil amendment, and so on. [10-12].

The performance of HTC process, and any transformation process, highly depends on transport phenomena, i.e., the mechanisms by which heat, mass, and momentum are transferred throughout a system, besides chemical reactions. The acknowledge of these phenomena in a reactor during HTC in a laboratory or pilot plant is tedious and expensive. For this reason, numerical simulation or Computational Fluid Dynamics (CFD) could be necessary and complementary to experimental studies. A better understanding of these phenomena, inside the HTC reactor at laboratory level, can facilitate their optimization and scale-up to a more accurate industrial reactor, which will reduce economic uncertainty. Compared to the experimental data, CFD model results can predict qualitative information and, most of the times, accurate quantitative information [13]. In this regard, many researchers have used CFD to simulate and

analyze thermochemical conversion equipment performance, such as fluidized beds, fixed beds, firing boilers, combustion furnaces, so one. Papadikis *et al* [14] use CFD modeling in fluid-particle interaction within a fluidized bed reactor in fast pyrolysis, the model was able to predict the residence time of the vapors and biomass particle inside the reactor, as well as the properties of the pyrolytic particle. On the other hand, Xue *et al.* [15] proposed a model able to predict the key features of fast pyrolysis of any biomass with known compositions of cellulose, hemicellulose and lignin in a fluidized bed reactor. Similar studies were reported by Thankachan *et al*.[16] on biomass gasification using a fluidized bed reactor. Kumar *et al.* [17] use CFD to investigate the syngas production of various biomass feedstocks. Hooshadaran *et al.* [18] studied the heat transfer in a draft tube conical spouted bed reactor under pyrolysis conditions. The CFD predictions results were in close quantitative agreement with measurements in terms of heat-transfer coefficients. Also, CFD has been used in gas-solid fluidized bed hydrodynamics studies [19, 20]; their models have been able to predict the hydrodynamic behavior of gas-solid fluidized beds. Xie *et al.* [21] showed the importance of CFD to understand the effects of agitation on the velocity, temperature, and concentration distributions of a stirred tank reactor and the importance of the stirring rate in copolymerization. In general, CFD has been used in many thermochemical conversion studies of biomass; however, there is minimal studies on the simulation of an HTC reactor and especially a stirred reactor. Most of the current simulation is based on the 0D kinetic model (without influence of spatial variables; the system behaves in the same way at any point of the reactor) [3, 22, 23]. All these studies assume that the reaction temperature is constant during the whole experiment, but a constant temperature during HTC is difficult to achieve in batch autoclave reactors where there is a heat-up time, a constant temperature period, and finally a cooling time. Therefore, the validity of these results depends only on their experimental conditions. Some investigators have incorporated the effects of heat-up time as in the case of Álvarez-Murillo *et al.* [24]. In this case, the authors applied the computational model by using COMSOL Multiphysics to examine the kinetics of cellulose HTC over different reaction times and temperatures. They developed a first order-reaction model based on the Arrhenius equation, which also shows the importance of the heating time. The authors reported activation energy of 90.1 kJ/mol similar value reported by Reza *et al.* [25] and Killer *et al.* [26], the latter not considering heat-up time. The CFD simulation carried out by Álvarez-Murillo *et al.* [24], considers batch HTC reactor that received heat from hot air and modelled radiation and

convection and under the assumption that the reactor contains only water, and does not consider the properties of biomass. However, the thermal properties of biomasses may differ from the thermal properties of water in the reaction medium. The biomass properties, such as density, porosity, permeability, and chemical composition change for unexplored chemical reactions [27]. Also, Funke and Ziegler [28], report that the global biomass HTC reaction is exothermic; therefore, the biomass-to-water ratio influences the heat transfer. According to Funke and Ziegler, the HTC reaction of biomass can release heat to -5.8 MJ/kg of fed biomass. For this reason, and as a remarkable difference regarding previous works, we have considered temperature as a function of time (t), spatial variables (x, y, z), and biomass-to-water ratio (R), given the difference between the thermal properties of biomass and water. Also, it is a stirred reactor, of constant volume and working in an open-loop controller system. To determine $T_{(t, R, x, y, z)}$ inside the reactor, the model resolves the mass, heat, momentum transfer, and reaction kinetics simultaneously. Besides, most of the HTC reactor studies in the literature are non-agitated reactors, and operated with furnace in a closed-loop system [4, 8, 9, 24]. In non-agitated reactors, the biomass/water mixture is not uniform inside the reactor, due the different physical properties of biomass and water (e.g. density). Consequently, a gradient of concentration, temperature and other properties may exist inside the reactor. These affect the mechanisms of reaction of HTC, also makes difficult their hydrodynamics analyses and thermal studies. The inclusion of a stirrer reactor can help avoid these problems, and the use of CFD simulation can contribute to the design, optimization, as well as the scaling up to industrial level. In addition, CFD can assist in the analysis of hydrodynamic and thermal effects inside the reactor during the HTC process.

Hence, the main objectives of this study were to use the CFD technique to produce a 3D simulation of HTC stirred reactor for an open-loop controller system by using COMSOL Multiphysics software: (a) to study the hydrodynamic and determine the distribution of biomass inside the reactor, high mixing intensity and stagnant zones. (b) to determine the heat of the reaction and the type of chemical reaction. (c) to combine kinetics, temperature, mass, and velocity fields to predict the conversion of the biomass inside the reactor using the model proposed by Álvarez-Murillo *et al.* [24], considering the thermal properties of the AS and heat of reaction, and the effect of biomass to water ratio on heat transfer. These results will be compared with the experimental data of the HTC of AS.

2 EXPERIMENTAL SECTION

2.1 Biomass feedstock properties

In this study, AS of the *Hass* variety from Michoacán (Mexico) were used. Mexico is the largest producer of avocado in the world, with 2.3million metric tons reported for the 2019/2020 marketing year [29]. A significant amount (~170,000 tons/year) of avocado production is processed as guacamole, this represents more than 25,000 tons per year of waste [30]. In general, the AS has a moisture content between 65 and 75% [31], which is ideal for HTC. The ultimate analysis and higher heating value (HHV) characteristic of raw AS is presented in **Table 1.** Initially, the AS was cut to obtain a particle diameter between 2.5 and 4mm and later dried in a stove at 80°C for storage.

Table 1: The ultimate analysis and HHV characteristic of the raw AS *Persea americana (Hass* variety) [32].

Ultimate analysis (%)	
Carbon	48.01±0.0079
Hydrogen	5.755±0.0158
Nitrogen	0.447±0.0566
Sulphur	0.104±0.0028
Oxygen	42.8±2.5738
Chlorine	0.024±0.0010
Ash	2.86±0.0167
HHV (MJ/kg)	19.15±0.1300
Oil content (%)	1.715±0.3540

2.2 HTC reactor description

The HTC experiments were carried out in a stirred autoclave reactor (Top Industrie, France). This reactor consists of two parts: a reactor vessel with an internal volume of 300 mL and a cylindrical capping vessel. The capping vessel includes a central connection for a magnetic stirrer (max. 1500 rpm, 50 W) and connections for measuring pressure, temperatures, and releasing the gases produced. The clamping of the reactor is done by opening and closing the cylinder head manually. The autoclave is placed in a furnace for electrical heating (maximum power is 400 W). During the experiments a constant electrical power of 120 W was applied. The geometry of the reactor is shown in **Figure 1a**. The reactor is mainly equipped with the following instruments: furnace control panel for on-line temperature control and display, Type-K thermocouples immersed inside the reactor; manometer, the agitator control box to regulate,

measure and display the stirring speed; and Huber Ministats® for water recirculation at 5ºC to cool the reactor.

2.3 HTC experimental procedure

HTC experimental runs were performed with four avocado stones (AS) to Water (W) ratios under the same operating conditions: residence time (8h), power supplied in the reactor (120 W), particle diameters between 2.5 and 4 mm, and agitator speed (550 rpm). For each experiment, it was used the same volume inside the reactor (200 mL). The biomass-to-water ratio (AS/W) was: AS-1-10 (18.74g/187.45g:AS/W), AS-1-8 (23.08g/184.68g:AS/W), AS-1-6 (30.04g/180.24g: AS/W), AS-1-4 (42.99g/171.98g: AS/W). To remove the residual air inside the reactor, vacuum conditions were applied to the reactor with a pump; after reaching a pressure of less than 40 mbar, the heating program was started. The heating period was 8 hours long. At the end of this period, the reactor was cooled to room temperature; it took 15 to 20 minutes to cool it down by immersing it in a 5°C water bath.

Thermal properties, such as thermal conductivity, specific heat capacity, as well as density, were determined for the AS and hydrochar. The thermal conductivity was determined following the protocol described by Mason *et al.* [33], the heat capacity of the samples was determined according to the protocol described by Blackman *et al.* [34]. For density, a pycnometer was used to determine the samples densities.

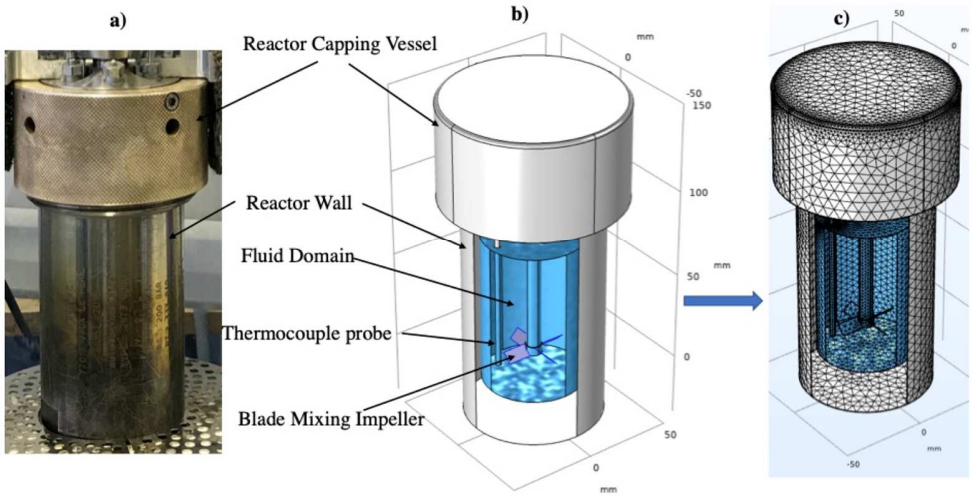

Figure 1: The reactor geometry **a**) experimental **b**) CFD domain and **c**) Meshed CFD domain

2.4 Heat of reaction measurements

The energy supplied to the external wall of the reactor during HTC is the sum of the energy used to heat the reactor, the room-temperature mixture to a final temperature and the energy lost in this heating over time (mostly at the reactor head), and is presented in the following equation:

$$E_S = E_R + E_w + E_{bi} - E_L \pm E_P \quad (1)$$

where E_S (kJ) is the power or energy supplied to the reactor, E_R (kJ) energy used to heat the reactor, E_W (kJ) energy used to heat the distilled water, E_{bi} (kJ) energy used heating biomass and E_L (kJ) the energy lost. If the decomposition of biomass produces or consumes energy, the term E_P (kJ) is the energy produced or consumed during chemical reactions. In our case, we opted to use an open-loop controller system in view to know the energy supplied. The power applied in each experiment is equal to 120 W.

(Complementary informations were given into **supplementary document**)

3 COMPUTATIONAL APPROACH AND METHODOLOGY

3.1 Geometry, Mesh and Solver settings

3.1.1 Geometry

The simulated stirred reactor comprises a reactor vessel and a four-blade impeller. The internal height (H) and the inner diameter (D) of the mixer vessel is 130 mm and 56 mm respectively. The diameter of the impeller (d) was 35 mm. The pitch of the impeller blades was 45°; the external width (Dex) was 76 mm. The details of the geometry are presented in **Figure 2**.

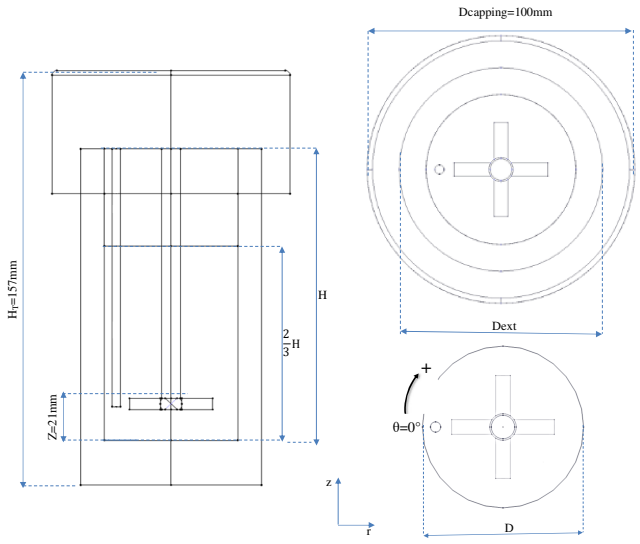

Figure 2: Stirred reactor geometry details schematic

The geometric models were constructed in the COMSOL Multiphysics. Simulations were performed on a Dell Studio XPS 9100 PC intel i7CPU with 16 GB memory.

3.1.2 Mesh independence study

Mesh independence study is one of the most crucial steps in any CFD problem. The accuracy of the CFD solution is strongly dependent on the mesh quality. When the accuracy does not change significantly with the increasing number of mesh elements, the calculation can be considered mesh independent [35]. It is important to mention that the agreement between simulation results and experimental data does not necessarily mean that the solution is mesh-independent. Achieving a mesh-independent solution is an essential step in analyzing the results obtained using CFD simulation. However, there is no specific method in the literature on how to achieve a mesh-independent solution [36]. In this case, it was used the average velocity of the dispersed phase for mesh-independence study. When this average velocity does not change with the increase of the number of elements, it was considered that the results are mesh-independent. Once the results are validated as mesh independent, it was validated with experimental data. Then, the CFD model can be used to design, scale-up, test, and process optimization. For this, six predefined meshes were applied. The variation of average velocity of the dispersed phase as a function of the number of elements as well as the computation time is presented in **Figure *3***.

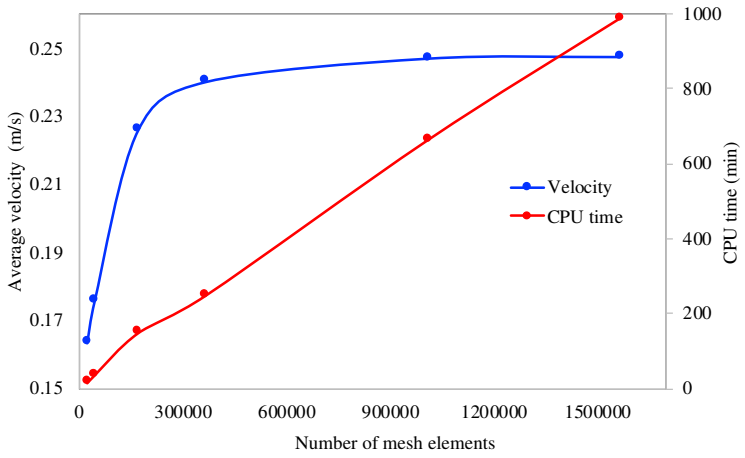

Figure 3 : Effect of number of mesh elements on average velocity of the dispersed phase and computation time

As shown in **Figure *3***, from 500k elements, the variation of average the velocity of the dispersed phase is negligible. This simulation takes a minimum of 500 k elements to consider the results are mesh-independent. The independent mesh study was conducted using an agitation speed

equal to 550rpm and fraction volume φ_b=0.1375. The reactor mesh domain is presented in **Figure 1c**.

3.1.3 Solver settings

For solver settings in rotating machinery, the mixture model (turbulent or laminar) interface supports the steps (stationary and time-dependent) of both types of studies. For time-dependent 3D simulations, it is critical to have an accurate initial value that corresponds to the real situation. To simplify the simulation, the velocity field was calculated using the frozen rotor assumption, a particular case of a steady-state study. The results were used as initial values for the time-dependent study.

3.2 Stirred reactor hydrodynamic simulations

In the mixing system analysis, Reynolds number (N_{Re}) is an important design criteria [37]. For stirred vessels, the flow is laminar for N_{Re} <10 and fully turbulent for $N_{Re}>10^4$ [38]. The Reynolds number is defined and calculated according to the following equations:

$$N_{Re} = \frac{N d^2 \rho}{\mu} \quad (2)$$

where d (m) is the diameter of the impeller, N (s^{-1}) the represents impeller rotational frequency, μ (Pa. s) is the dynamic viscosity of the mixture, and ρ (kg/m^3) is the density. To study the dispersion or suspension behavior within the fluid, it is considered a diluted system in which the dispersed phase is rigid spheres, and the continuous phase is a Newtonian fluid. The continuous phase viscosity variation of a dispersed phase is described by Einstein's equation [39]:

$$\mu = \mu_0 \left(1 + \frac{\varphi_{bi}}{\varphi_{bi}^{max}}\right)^{2.5\varphi_{bi}^{max}} \quad (3)$$

where μ_0 (Pa. s) is the continuous phase viscosity, φ_{bi} (-) is the volume fraction of biomass particles in the dispersed phase, and φ_{bi}^{max}(-) is considered equal to 0.63 [40]; this is the maximum packing volume fraction. The mixture density is calculated from the following equation:

$$\rho = \rho_b \varphi_{bi} + \rho_c (1 - \varphi_{bi}) \quad (4)$$

where ρ_b (kg/m^3) is the density of the disperse phase, and ρ_c (kg/m^3) is the continuous phase density. Five rotation frequencies were used: 100, 250, 400, 550, and 700 rpm to find the ideal speed for the system to be homogeneous. The N_{Re} values at different volume fractions

corresponding to the different biomass to water ratios are presented in **Table 2** at 25°C. All N_{Re} values obtained are higher than 10; therefore, no regime is laminar. The regime is entirely turbulent for N=550 rpm and N=700 rpm, the decision is to use the turbulent regime and also, as the temperature increases, the N_{Re} value increases for constant N.

In all numerical analysis, particularly those using Reynolds-Averaged-Navier–Stokes (RANS) equations, the results accuracy depends on the turbulence flow models used [41]. This turbulence flow will be modeled using the k-ε turbulence model. This model can handle various fluid flow conditions, it is the most common model used in CFD to simulate mean flow characteristics for turbulent flow conditions, due to its good convergence rate and relatively low memory requirements **[**42**].**

Table 2: N_{Re} values at different rotation frequency and different biomass water ratio

Rotation frequency (N)	Reynolds number				
	Water φ_{bi} =0	AS-1-4 φ_{bi}=0.1375	AS-1-6 φ_{bi} =0.0961	AS-1-8 φ_{bi} =0.0738	AS-1-10 φ_{bi} =0.0600
100 rpm=1.67 s^{-1}	2291.43	1881.88	1983.27	2044.60	2085.26
250 rpm=4.17 s^{-1}	5728.58	4704.71	4958.18	5111.50	5213.16
400 rpm=6.67 s^{-1}	9165.73	7527.54	7933.09	8178.39	8341.06
550 rpm=9.17 s^{-1}	**12602.88**	**10350.36**	**10908.00**	**11245.29**	**11468.95**
700 rpm=11.67 s^{-1}	25043.44	20790.72	21843.53	22480.33	22902.60

It is not feasible to simulate directly the movement of all biomass individual particles in the HTC reactor due to the limitations of current computers and the high computational cost of tracking thousands of particles present in typical reactors. Thus, approximate methods, such as the dispersed multiphase flow models approach or coupling fluid flow and transport of diluted species, are ways to reduce computational overheads. Recently, these approximate methods were used by many researchers to study the hydrodynamics of the gas-solid during pyrolysis and combustion [15, 20, 43, 44].

3.3 Reactor simulations in HTC condition

The geometry of the reactor simulated is shown in **Figure 1b.** Inside the reactor, water and biomass are mixed in the function of biomass-to-water ratio. The thermal properties of the reactor and continuous phase (water) inside the reactor and its relationship with temperature were taken from the COMSOL Multiphysics database. The thermal properties of the biomass

determined in **section 2.3** were used. The fluid was considered weakly compressible to take into account variations in fluid density for temperature change. Since the system is closed, the pressure point was constraint.

The equations used for this simulation are presented into **supplementary document**.

3.3.1 Kinetics models

In this kinetic simulation of HTC, the kinetic model proposed by Álvarez-Murillo *et al.* [24] was used, with the modification of adding heat of the reaction of the HTC, calculated experimentally. The behavior of each biomass during the HTC process is related to its content in the constituent biopolymers (cellulose, hemicellulose, and lignin). However, the decomposition kinetics of this biopolymer for all types of biomass may be similar. The overall reaction of biomass in the HTC process is presented in the following reaction:

$$\text{Biomass} + H_2O \rightarrow \text{Hydrochar} + \text{Liquid} + \text{Gas} \qquad \Delta H_r \tag{5}$$

$$r_{bi} = -\frac{dC_{bi}}{dt} = K_1 . C_{bi} \tag{6}$$

$$K_1 = \left[\left[\frac{T_{(t,R)}}{T_{ref}}\right]^n e^{\left[\frac{-Ea}{Rg T_{(t,R)}}\right]}\right] . A_0 \qquad T_{ref} = 1K \tag{7}$$

This is an extension of Arrhenius equation in which the pre-exponential factor is proportional to T^n where $T_{(t,\ R)}$ is temperature (K) as a function of time, biomass concentration and spatial variables and n is a constant, A_0 (1/s) is temperature-independent constant, Ea (J/mol) is activation energy and Rg (8.314 J mol/K) is the constant gas, C_{bi} (kmol/m^3) is the biomass molar concentration inside the reactor, and r_{bi} (mol/m^3. s) rate of each reaction.

$$V_r \left[\sum_i C_{bi}\, C_p \frac{dT}{dt} + \sum_i H_{bi}\, r_{bi}\right] = Q_{ext} \tag{25}$$

$$r_{bi} = R_{bi} F_{bi} \tag{8}$$

The hydrochar formation kinetics is represented by:

$$r_{HC} = R_{bi} . (F_{Hc}) \tag{9}$$

And liquid formation kinetics as:

$$r_{liq} = R_{bi} . (F_{liq}) \tag{10}$$

Where Vr (m^3) is the reactor volume, Q_{ext} (W) external heat rate, H_{bi} (J/mol) enthalpy of each reaction, R_{bi} (mol/m^3. s) is the reaction rate for species i of biomass. F_i (-) is the fraction of

biomass converted into products, F_{HC}, F_{liq} is the fraction of the biomass converted into hydrochar and liquid respectively, these values were determined experimentally. The biomass fraction converted in to gas is represented as (1- F_{HC}-F_{liq}).

3.3.2 Boundary conditions

Initial conditions were: T=25°C, p=0 in the pressure point constraint, and u=0 throughout the system. An electrical power of 120 W was applied to the external reactor sidewall. No-slip boundary conditions (u=0) were applied at all solid/fluid interfaces. Natural external convection conditions were applied to the upper and lower sides of the reactor. There was a heat loss due to a faulty reactor insulation. The insulator heat transfer coefficient was determined from following equation:

$$h = \frac{q_0}{T_{ext} - T} \quad (11)$$

where h is the heat transfer coefficient (W/m^2K), T_{ext} (K) is the external temperature and q_0 (W/m^2) represents heat flux loss.

4 RESULTS AND DISCUSSION

4.1 Experimental feedstock analysis

4.1.1 Analysis of AS and hydrochar thermal properties

The experimental thermal properties values obtained, such as specific heat capacity, thermal conductivity, and initial biomass density of (AS) and the hydrochar (HC) produced, are presented in **Table 3**.

Table 3: Heat capacity and thermal conductivity of AS and hydrochars

Samples	Heat capacity (J/kg.K)	Thermal conductivity (W/m.K)	Density (kg/m^3)
AS	1518.17±3.79	0.1038 ±0.0039	1547.64±27.33
HC	1188.51±22.06	0.1100±0.0018	644.23±8.17

The heat capacities of the AS and its hydrochar are 1518.17±3.79 and 1188.51±22.06 (J/kg.K), respectively, similar values are commonly found on biomass and char in literature [45, 46]. Dupont *et al.*[45] studied the heat capacity of different biomasses, obtaining values between 1302 and 1822 J/kg.K in a temperature range between 40 and 80°C. Regarding char, Gupta *et al.*[46] found values ranging from 768 J/kg.K at 40 °C to 1518 J /kg.K at 440 °C; this is in

agreement with Raznjevik's [47] findings on charcoal. Many materials thermal conductivity is temperature-dependent, and biomass is no exception. Ragland *et al.* [48] reports that the wood thermal conductivity increases with temperature, finding values between 0.087 W/m.K at 25°C and 0.099 W/m.K at 100°C. In addition, the values almost follow a linear pattern. The authors report that wood thermal conductivity increases by 10% for every 50°C increase in temperature. For a temperature increase from 147 to 302 °C, Milosavljevic *et al.* [49] have reported thermal conductivity values for virgin cellulose pellets to increase from 0.050 to 0.070 W/m.K. Similar values were found by Gupta *et al.* [46] for softwood, softwood bark and softwood char of 0.099, 0.095 and 0.205W/m.K respectively. These values are similar to the values obtained in this study. As it can be observed in **Table 3**, heat capacity and thermal conductivity do not vary consistently from hydrochar and raw biomass. However, the density varies from 1547.64 ± 27.33 kg/m^3 for raw biomass and 644.23 ± 8.17 kg/m^3 for hydrochar. The biomass particles density could influence the heat transfer inside the HTC reactor. For example, if the particles are denser than water, the particles will settle at the bottom of the reactor, if they are less dense than water, they would float at top of it, this could cause non-homogeneity inside the reactor and, consequently, the heat transfer within the reactor will not be carried out correctly. Stirring helps to obtain a homogeneous mixture, avoiding sedimentation and flotation of the biomass particles.

4.2 Hydrodynamics

4.2.1 The effect of stirring speed.

The primary objective in mixing is to achieve a homogenous mixture; generally, this means, attaining a nearly uniform distribution of the ingredients, in this case the uniform distribution of AS particles inside the reactor. To find the ideal speed for the system to be homogeneous. The criterion we set for considering the particles as uniformly distributed was based on the Reynolds number (**Table 2**). If the regime is turbulent, it was considered that the particles are distributed uniformly inside the reactor. **Figure 4** shows the velocities contours for different impeller speeds in the same initial volume fraction (φ_b=0.1375). The impeller speed varies between 100 and 700 rpm. In the mixture between solid and fluid particles, two main forces govern the flow velocities in the agitator, inertial forces that result from the rotation of the impeller and dispersed-phase buoyancy forces, or hydrostatic force which result from density differences between the phases.

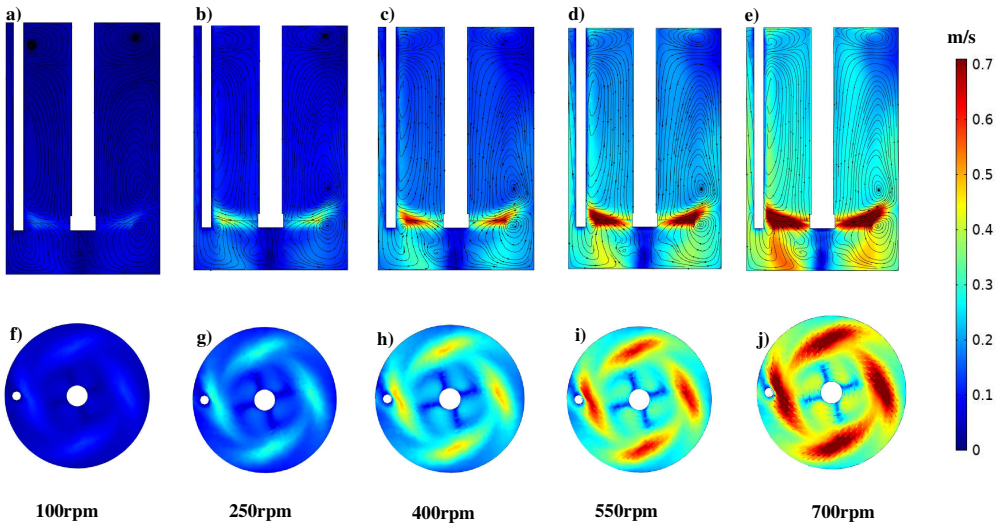

Figure 4 : The effect of the stirring rate on the volume fraction φb=0.1375: **a-d**) r-z plane defined by the angular coordinate θ = 0° and **e-h**) r-θ plane defined at the top of the impeller for z=21mm

For N=100 rpm, in **Figure 4a** and **Figure 4f**, no agitation effect is observed, the flow velocity is practically null inside the entire reactor. The average velocity in the dispersed phase is 0.03m/s. The same tendency is observed for N=250 rpm, and the flow velocity variation is only observed in the impeller zone where the maximum velocity is less than 0.15m/s and average velocity is 0.09m/s (**Figure 4b** and **Figure 4g**). For N=400 rpm, a high velocity starts to be observed at the bottom of the reactor (**Figure 4c** and **Figure 4h**). However, on the top of the reactor, the flow velocity is still controlled by gravity or hydrostatic force and average velocity is 0.16m/s. In **Figure 4d** and **Figure 4i,** it seems that a uniform distribution of particles is observed inside the reactor. The highest velocities vectors are in an upward direction, except in regions just below the impeller shaft. Therefore, it can be concluded that the predominant forces for the movement of particles inside the reactor are the inertial forces. The hydrostatic force has no significant effect on the movements of the particles for N=550 rpm, corresponding to a Reynolds number value superior to 10^4 meanings a turbulent regime. From this speed, the regime is completely turbulent, as shown in **Table 2**. The average velocity in the dispersed phase is 0.24 m/s. This velocity can be considered as ideal velocity to achieve a uniform distribution of the particles inside the reactor. The same phenomenon can be seen in **Figure 4e** and **Figure 4j** for N=700 rpm.

The higher rotation speed reduces the volume fraction dispersion time from the bottom to a uniform distribution inside the reactor, and increase the reaction mechanisms in the HTC process,

however, the increased rotation speed is associated with higher energy consumption. Therefore, reaching a compromise between the energy consumption of the agitator and the homogenization of the volume fraction inside the reactor is necessary. For a relatively high speed (550 rpm), the reactor can be considered perfectly homogeneous. For the experimental studies it was used a rotation speed of N=550 rpm creating a homogeneous system inside the reactor, and a turbulent regime ($N_{Re}>10^4$).

4.2.2 Validation of the flow velocities

The results of any simulation are useful when they are validated with experimental data. To ensure that the CFD models are reliable to describe hydrodynamics inside the HTC reactor, a simulation was performed using only water. The axial and tangential velocities were validated with experimental curves from Özcan-Taşkin and Wei [50]. Özcan-Taşkin and Wei determined the fluid velocities using Laser Doppler Anemometry (LDA) measurements with a pitched-blade turbine agitator. In this CFD simulation, a k-ε turbulent model was used, the same model used by Özcan-Taşkin and Wei for their simulation. In a cylindrical reactor coordinate system, velocity at any point can be decomposed into its radial, axial and tangential values. The axial and tangential velocities results were compared with experimental data. The velocity results were obtained in a stationary state (frozen rotor). The axial coordinates r-θ is located just on the top of the impeller for z=21 mm and tangential plane r-z for θ=0° rotation angle. The results obtained are presented in **Figure 5**.

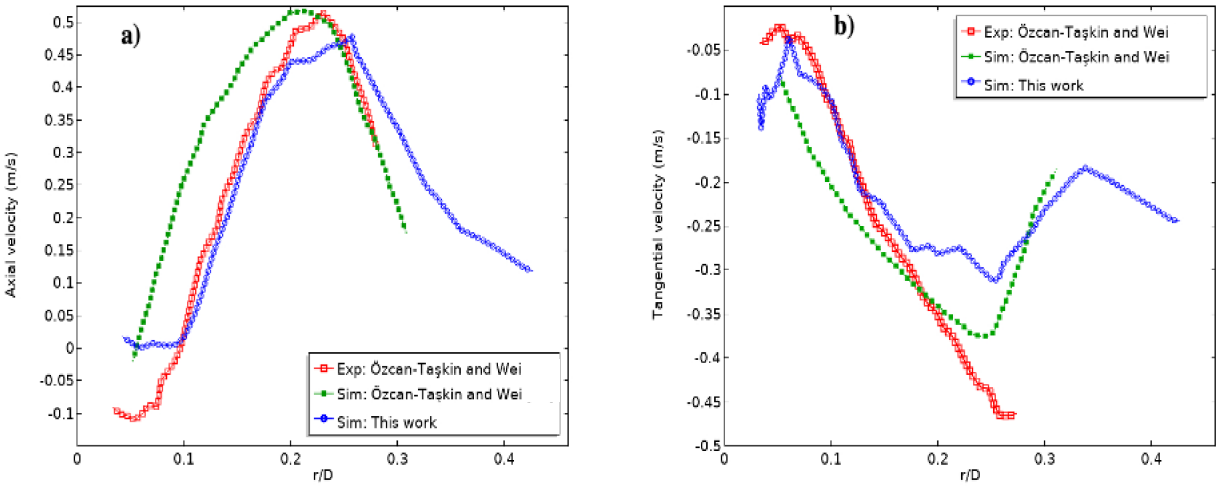

Figure 5 : Comparisons of a) Axial velocity for z=21mm and b) tangential velocity for θ=0° in this simulation with previous works

The CFD results show the same tendency of axial and tangential velocity distribution with the experimental data, which means that the simulations could capture the general characteristics of the flow field inside the reactor during the HTC process. Once the model was validated with experimental data, the simulations were carried out with a different fraction volume according to the experimental data used in this work.

4.2.3 Comparison of flow velocity for pure water and with biomass -to-water mixture.

In this simulation, the flow velocity for pure water and water with volume fraction equal to φ_b=0.1375 was compared at a rotation speed N=550 rpm. **Figure 6**, the flow patterns of primary velocity vectors on the impeller top for z=21 mm are shown in **Figure 6a-b** in the r-θ plane and the secondary flow in the r-z plane for θ=0° on the **Figure 6c-d.**

There is no difference between the velocity vectors in the r-θ plane at z=21 mm. In the secondary flow, the r-z plane, recirculation zones are observed; up and down the impeller, the usual double-loop flow structure corresponding to radial impellers can be observed in both r-z planes (**Figure 6a-b).** However, in the r-z plane, in the (**Figure 6b**), an additional recirculation zone is observed at the top of the reactor. In this area, the flow velocity is higher and varies between 0.25 and 0.3 m/s; this may be due to dispersed-phase buoyancy forces of some particles. On the other hand, in the reactor with water (**Figure 6a**), this recirculation zone at the top of the reactor is not observed, the velocity is lower and it varies between 0.1 and 0.15 m/s.

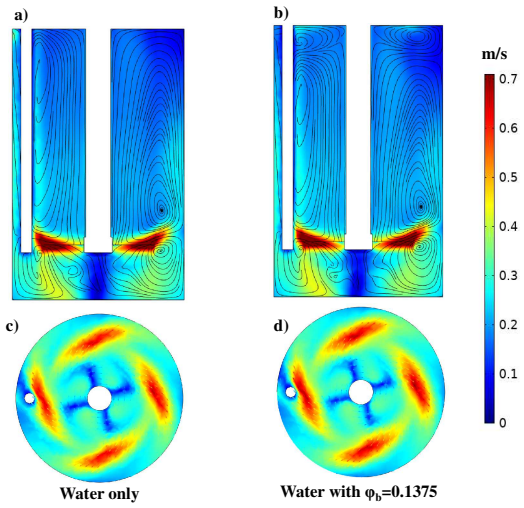

Figure 6: Distribution of turbulent flow velocity induced in a, b) r–z plane for θ = 0° and c, d) r–θ plane on the impeller top for z=21mm, and N=550 rpm

The flow velocity is strongly dominated by the rotational component in the area near the impeller, where the flow velocity varies between 0.6 and 0.75 m/s. Also, it can be seen that the thermocouple probe also disturbs the flow velocity in the tangential direction (**Figure 6c-d**). Below the impeller, there are stagnant areas inside the reactor, where the flow velocity varies between 0 and 0.05 m/s. This stagnation may be due to the perpendicular flow of the impeller, which could maintain the low velocity in this area.

4.2.4 Flow and solid distributions.

The homogeneous distribution of the solid particles inside the reactor is the main objective of agitation. This subsection shows a simplified CFD model implemented to understand the system. It is also necessary to have a more realistic model that accounts for solid and their distribution inside the reactor; by observing region stagnation, it may be possible to improve the reactor design. **Figure 7** shows a cross-section of the contours of the volume fraction φ_b=0.1375 at 550 rpm in the reactor at 0s, 0.1s, 1s, and 5s. Initially, the solids are found at the bottom of the reactor, owing to the density of the particles of AS and gravity. The red color indicates the dispersed phase or the biomass concentration, while the blue color shows the continuous phase or absence of the solid particles. The AS particles are not entirely spherical; therefore, the maximum volume fraction was determined experimentally and corresponded to φ_b=0.52. For reference, the maximum packing volume fraction would be 0.63 if the particles were spherical [40].

At 0s, the major concentration of biomass is at the bottom and represents a φ_b=0.52, and at the top, the volume fraction φ_b=0, as shown in **Figure 7a,e.** Although particles are not completely spherical, it was observed that they packed up effortlessly at the bottom of the reactor owing to their higher density than water.

At 0.1s, the impeller moves most of the solids into the reactor wall, as shown in **Figure 7b,f.** This is due to the agitation force, which pushes the particles away from the impeller. However, regions of higher volume fractions of the dispersed phase are also observed at the bottom of the reactor and the sidewalls near the impeller.

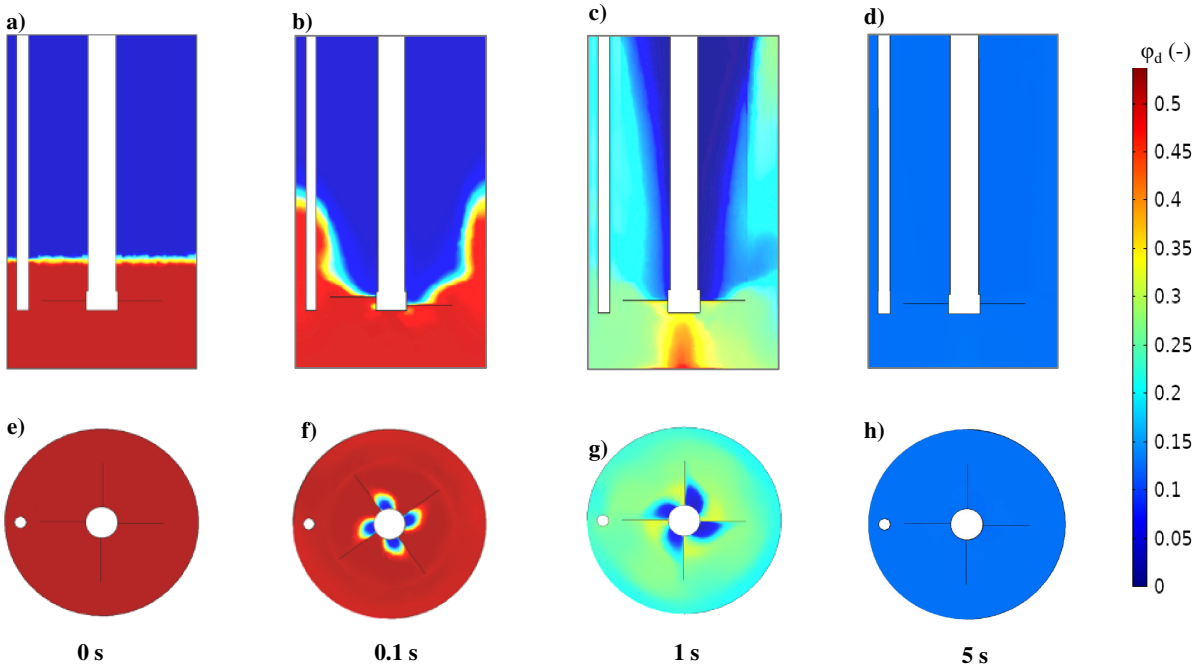

Figure 7: Two-phase CFD simulation of volume fraction φ_b=0.1375 on water: the rheological distribution: **a-d**) induced in the r-z plane defined by the angular coordinate θ = 0° and **e-h**) in the r-θ plane defined at the top of the impeller for z=21mm, and N=550 rpm

As shown in **Figure 7c,g,** at 1s of agitation time, the impeller moves most of the particles to the top and to the reactor walls the volume fraction is between 0.2 and 0.3. However, near the impeller shaft, the center of the reactor is the least agitated zone, and so there can be found the most concentrated part of the volume fraction. Below the impeller, there are stagnant areas inside the reactor, as explained in **section 4.2.3.** At 5s, as shown in **Figure 7d,h,** the reactor is wholly mixed, and the volume fraction in the dispersed phase is 0.1375 everywhere inside the reactor. Little time was needed to obtain a homogeneous mixture inside the reactor with a 550 rpm speed.

4.3 Temperature profiles inside the HTC reactor

As explained in **section 4.2.4,** the volume fraction in the dispersed phase is completely homogeneous inside the reactor after 5 seconds of stirring. Thus, agitation was not considered in this part of the simulation to reduce the computation time, and we can consider that the particles are entirely distributed within the reactor. The experimental temperature profile data was also used to validate the CFD simulation.

To validate the simulation with experimental data, the insulator heat transfer coefficient of **Equation** (11) has to be determined. The average heat-transfer coefficient (h) in the insulation to the environment was estimated using experimental data values recorded during the water heating (**Figure 8a**) under HTC conditions. Different values of heat-transfer coefficient were used in **Equation** (11) in order to match the simulated curve with the experimental one, based on a constant heat flow (120 W) over the external surface of the reactor. The average heat transfer coefficient that best fits the experimental data is 11.66 $W/m^2.K$. This value was used to set the heat loss during the HTC process of different biomass-to-water ratios in the CFD simulation. The thermal properties of AS determined in **Table 3** were used, as well as the thermal properties of water. These data allowed the simulation of the temperature profile evolution according to the volume fraction used.

The results in **Figure 8b** show that there is practically no difference between the experimental temperature profile of water and the modeling temperature profiles with different volume fractions of biomass. The maximum temperature difference observed is less than 3°C; this difference can be considered negligible. However, experimentally, there is a significant difference between the water temperature profile with different volume fractions of biomass as shown in **Figure 8b.** The most notable difference is 21.42°C, and it was observed for the higher volume fraction of biomass (φ_b=0.1375), this difference is decreasing to 6.87°C for φ_b=0.06. These variations are essential, considering that temperature is the main factor that controls the HTC process. Also, this variation begins to be observed from 150°C, as shown in **Figure 8b.**

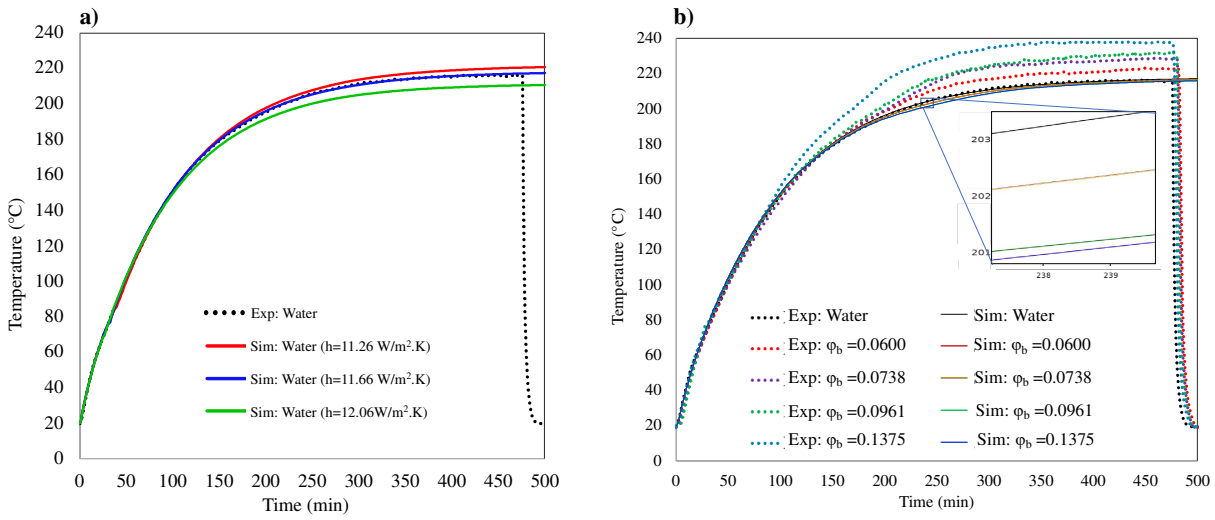

Figure 8: a) Determination of the heat-transfer coefficient between the insulator and the environment; **b)** Comparison of simulated and experimental data using the thermal properties of biomass

There are indeed differences between the thermal properties of biomass and saturated water in the HTC condition; however, this difference is not significant to observe a variation in temperature up to 21.42ºC. With CFD simulation, using the biomass thermal properties for the different volume fractions, the difference between profiles temperature calculated was less than 3 ºC. Furthermore, if the temperature variation is the result of the difference between the physical properties of water and biomass, this variation would be noticed from the beginning of the heating process, and not from 150ºC, where the main components of biomass start to decompose [45, 46, 51]**.** Only chemical reactions can cause temperature variation from 150ºC to the equilibrium temperature. It can be stated that the overall reaction of avocado stone HTC is exothermic, and also, the biomass to water ratio influences the heat transfer, therefore the reaction kinetics.

4.4 Heat of reaction and biomass to water ratio effect on heat transfer.

The results of the energy produced in each of the biomass-to-water ratios are presented in **Table 4**. It can be seen that, when the biomass-to-water ratio is increased, the heat produced increases, and consequently, the temperature inside the reactor increases. As the concentration of biomass increases, there is a high probability that more exothermic reactions will occur inside the reactor. For example, for the AS-1-10 (φ_b=0.06), the total reaction heat released during 8 hours of heating was 135.7kJ, while at the same time, the AS-1-4 (φ_b=0.1375) released 298.5kJ. Therefore, the higher biomass-to-water ratio favors the heat transfer of HTC reaction. The heat

of the reaction produced at an average temperature of 215°C during 8 hours of HTC is -7.25 ±0.32MJ/kg of feedstocks. Similar values were reported by Merzari *et al.* [52], -7.3 MJ/kg feed at 220 °C of organic fraction of municipal solid waste and residence time of 3 hours. Additionally, Funke *et al.*[28], reports values for glucose equal to -5.8 MJ/kg feed.

Table 4: Experimental results of the heat produced for different biomass-to-water ratios of AS

Biomass-to water ratio	Heat released (kJ)	Reaction heat (kJ/kg of feed)
AS-1-10	135.72	7261.96
AS-1-8	179.67	7740.70
AS-1-6	212.22	7065.25
AS-1-4	298.50	6944.25

It can be concluded that the global HTC reaction is exothermic. The exothermic character of the HTC reaction found here is in agreement with that reported by Funke *et al.*[28] and Merzari *et al.* [52]. It is also important to mention that the biomass-to-water ratio has an effect on heat transfer during the HTC process.

4.5 Temperature profiles inside the HTC reactor using kinetic parameter and model validation with experimental data

Most of the kinetic models reported in the literature for the biomass HTC process are dimensionless models, i.e., no influence of spatial variables; the system behaves the same way at any point in the reactor, constant temperature, and no influence of biomass concentration inside the reactor. However, Álvarez-Murillo *et al.* [24] proposed a model that incorporates the heat-up time, but his model is independent of the biomass concentration.

Initially, to determine the temperature profiles inside the reactor, the model proposed by Álvarez-Murillo *et al.* [24] was used. However, this model was unable to reproduce the temperature profiles inside the reactor during the HTC of AS because the model is biomass concentration independent. The model proposed by Álvarez-Murillo *et al*. is incomplete because the overall reaction of the HTC is exothermic. In this context, we decided to use the reaction heat, which depends on the biomass concentration. **Figure 9a-d** shows the results of the models proposed in this work. The results of the CFD simulation temperature profiles were validated

with experimental data in different volume fractions. The initial condition and kinetic parameters used for this simulation are presented in **Table 5**.

Table 5: The values used for the kinetic study

Biomass-to water ratio	Initial condition			Product	
	Biomass volume in reactor (mL)	Water volume in reactor (mL)	volume fraction φ_b (-)	F_{HC}	F_{Liq}
AS-1-10	11.99	188.01	0.0600	0.42	0.55
AS-1-8	14.77	185.23	0.0738	0.48	0.47
AS-1-6	19.22	180.78	0.0961	0.50	0.44
AS-1-4	27.50	172.50	0.1375	0.52	0.42
Density of AS	1548 (kg/m^3)	The total volume of each experiment was 200mL			
Heat of reaction of AS	-7.25 (MJ/kg of feed)	Kinetic parameters			
Molar mass of AS [32][a]	96.59 (kg/kmol)	E_a=90.1 kJ/mol[b]	n=2.2[b]	A_0=0.55 s^{-1}	

[a] Molar mass was determined from elemental analysis of AS

[b] The kinetic parameters taken in the Álvarez-Murillo *et al.* [24] model

The CFD simulation reproduces reasonably well, the temperature profiles for volume fraction φ_b=0.06; φ_b=0.0738 and φ_b=0.0961 (**Figure 9a-c**). However, for φ_b =0.1375 (**Figure 9d**) after 360 minutes of heating, the temperature profile reaches a maximum and starts to decrease. It seems that the exothermic reactions are over; the temperature profile tries to return to the equilibrium temperature, which is 215°C, due to the loss of energy. The temporal evolution of the temperature inside the reactor, different products relative mass yield (total solid or hydrochar, liquid, and gas) are shown in **Figure 9a-d.** Three zones can be noted in these CFD. simulation figures for the relative mass yield of volume fraction of AS. In the first zone, there is a horizontal period up to 150°C, which could be called induction; in this zone, no decomposition of avocado stone is observed. This initial non-reactive period would be explained by the existence of the heating ramp inside the reactor. In this period, the temperature is not high enough to reach an energy level that allows the activation energy. The reaction starts at a temperature of ~150°C. This observation is in line with the experimental data, where from 150°C, the temperature profile variation between the water and the different biomass volume fractions is observed. It is important to note that from 150°C, the HTC reaction starts; this confirms the importance of taking into account the heat-up time and not only the temperature fixed period during the

experiments for the kinetic models, the same phenomenon was also observed by Álvarez-Murillo *et al.* [24].

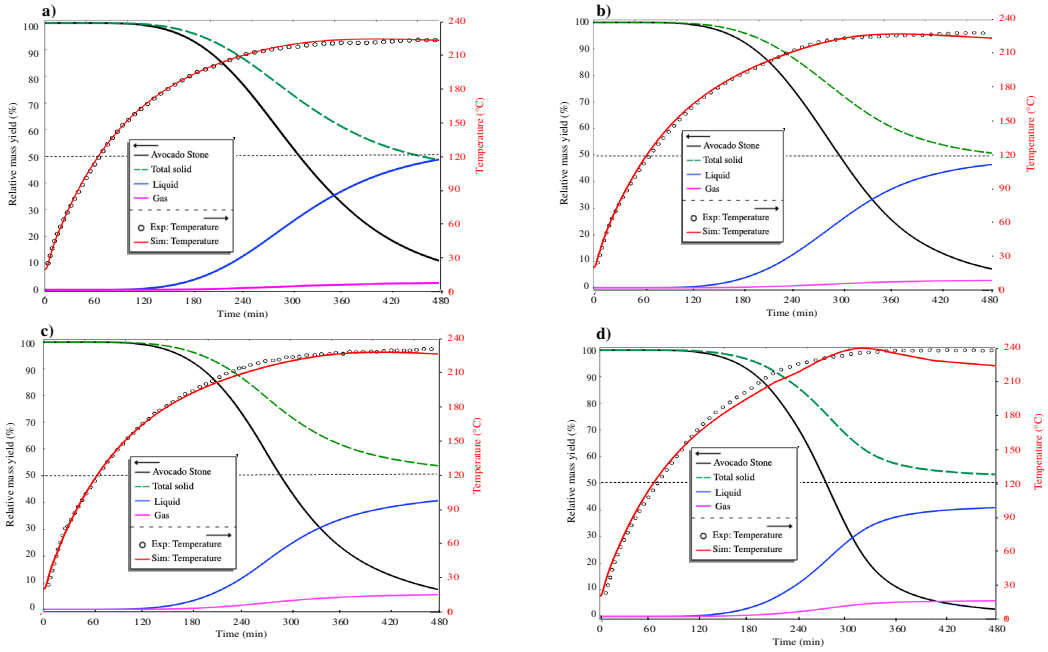

Figure 9: Temperature profiles and relative mass yield on different HTC products, using the reaction heat

Figure 9a shows that the maximum amount of total solid or hydrochar inside the reactor is 45% in this simulation; a similar value was obtained experimentally 42%. However, the reaction does not seem to end. The same behavior can be observed in **Figure 9b.** In **Figure 9c-d**, although the temperature inside the reactor is higher, the mass yield is higher than the lower biomass to water ratio (**Figure 9a-b**). Finally, it is observed that in the **Figure 9a-c**, there is still a small quantity of the AS (~10%) that has not yet reacted, this is due to the high value of the activation energy (90.1 kJ/mol), showing that these reactions are not over.

5 CONCLUSIONS

This work was focused on CFD modeling of hydrodynamics, heat transfer, and kinetics reactions of the HTC process of AS using a stirred reactor fitted with an open-loop controller system. The mass, heat, and momentum transfer equations, including kinetics reactions, were solved simultaneously to simulate the temperature profile $T_{(t, R)}$ and the evolution of the relative mass

yield of the different products (total solid, liquid, and gas). The following conclusions can be drawn from the results of the study:

The hydrodynamic study shows that the ideal stirring speed to obtain a homogeneous mixture inside the reactor is 550 rpm, given a turbulent regime, and the average velocity corresponding to the dispersed phase is 0.24m/s, owing to AS particles high density. At this stirring rate, the predominant forces for the movement of the particles inside the reactor are the inertial forces. For a lower stirring speed, the hydrostatic force predominates in the movement of the particles.
The application of CFD simulation allowed the model construction that describes the heat transfer inside the reactor during the HTC of the AS. The model considers the reactor heat-up time, inside the reactor biomass concentration, and the water thermal properties evolution and the thermal properties of biomass during the HTC process. The good fit to the experimental data gives this model the validity to predict the process behavior for specific experimental conditions. This model is general and can be used for any biomass with the known kinetic parameter and ultimate analysis. The CFD simulation results show that the difference between the thermal properties of biomass and water under HTC conditions is negligible. The global HTC reaction is exothermic; the heat produced is -7.25 ±0.32MJ/kg of feed. The biomass-to-water ratio has an effect on heat transfer during the HTC process. It is crucial to consider the biomass concentration in the kinetic model of the HTC process and heat-up time. The reaction starts at 150°C. Also, it is observed that the mass yield is bigger for the higher biomass to water ratio; from an energetic point of view this acquires certain importance, because the more biomass inside the reactor, the more hydrochar is obtained. The present modeling approach thus shows a promising way to simulate biomass HTC processes on an industrial scale.

Acknowledgments

The authors are grateful to CONACYT (Consejo Nacional de Ciencia y Tecnología de México) for granting the scholarship No. 659624 for this research. Also, we are grateful to ICARE - CNRS- France and the Région Centre-Val de Loire for financial support within the INFLUX project.

References

1. Ruiz J A, Juárez M, Morales M, Muñoz P, Mendívil M. Biomass gasification for electricity generation: Review of current technology barriers. Renewable and Sustainable Energy Reviews 2013; **18**: 174-183.

2. Kumar S, Ankaram S, Waste-to-Energy Model/Tool Presentation, in Book Waste-to-Energy Model/Tool Presentation. 2019, Elsevier.

3. Baratieri M, Basso D, Patuzzi F, Castello D, Fiori L. Kinetic and thermal modeling of hydrothermal carbonization applied to grape marc. 2015.

4. Missaoui A, Bostyn S, Belandria V, Cagnon B, Sarh B, et al. Hydrothermal carbonization of dried olive pomace: Energy potential and process performances. Journal of Analytical and Applied Pyrolysis 2017: 281-290.

5. Thrän D. Smart Bioenergy: Technologies and concepts for a more flexible bioenergy provision in future energy systems. 2015.

6. Chen W-H, Ye S-C, Sheen H-K. Hydrothermal carbonization of sugarcane bagasse via wet torrefaction in association with microwave heating. Bioresource technology 2012; **118**: 195-203.

7. Zhang L, Liu S, Wang B, Wang Q, Yang G, et al. Effect of residence time on hydrothermal carbonization of corn cob residual. BioResources 2015; **10**(3): 3979-3986.

8. Sabio E, Álvarez-Murillo A, Román S, Ledesma B. Conversion of tomato-peel waste into solid fuel by hydrothermal carbonization: Influence of the processing variables. Waste management 2016; **47**: 122-132.

9. Álvarez-Murillo A, Román S, Ledesma B, Sabio E. Study of variables in energy densification of olive stone by hydrothermal carbonization. Journal of Analytical and Applied Pyrolysis 2015; **113**: 307-314.

10. Ding L, Wang Z, Li Y, Du Y, Liu H, et al. A novel hydrochar and nickel composite for the electrochemical supercapacitor electrode material. Materials Letters 2012; **74**: 111-114.

11. Fernandez M E, Ledesma B, Román S, Bonelli P R, Cukierman A L. Development and characterization of activated hydrochars from orange peels as potential adsorbents for emerging organic contaminants. Bioresource technology 2015; **183**: 221-228.

12. Kladisios P, Sagia A. Hydrothermal carbonization: production of energy through the thermochemical treatment of biomass. SUSTAINABLE ENERGY VOL. 9, NO. 2 2018.

13. Wang Y, Yan L. CFD studies on biomass thermochemical conversion. International journal of molecular sciences 2008; **9**(6): 1108-1130.

14. Papadikis K, Gu S, Bridgwater A. CFD modelling of the fast pyrolysis of biomass in fluidised bed reactors. Part B: Heat, momentum and mass transport in bubbling fluidised beds. Chemical Engineering Science 2009; **64**(5): 1036-1045.

15. Xue Q, Heindel T, Fox R. A CFD model for biomass fast pyrolysis in fluidized-bed reactors. Chemical Engineering Science 2011; **66**(11): 2440-2452.

16. Thankachan I, Rupesh S, Muraleedharan C. CFD Modelling of Biomass Gasification in Fluidized-Bed Reactor Using the Eulerian-Eulerian Approach. in Applied Mechanics and Materials. 2014. Trans Tech Publ.

17. Kumar U, Paul M C. CFD modelling of biomass gasification with a volatile break-up approach. Chemical Engineering Science 2019; **195**: 413-422.

18. Hooshdaran B, Hosseini S, Haghshenasfard M, Esfahany M N, Olazar M. CFD modeling of heat transfer and hydrodynamics in a draft tube conical spouted bed reactor under pyrolysis conditions: Impact of wall boundary condition. Applied Thermal Engineering 2017; **127**: 224-232.

19. Ahuja G, Patwardhan A. CFD and experimental studies of solids hold-up distribution and circulation patterns in gas–solid fluidized beds. Chemical Engineering Journal 2008; **143**(1-3): 147-160.

20. Hosseini S H, Ahmadi G, Rahimi R, Zivdar M, Esfahany M N. CFD studies of solids hold-up distribution and circulation patterns in gas–solid fluidized beds. Powder technology 2010; **200**(3): 202-215.

21. Xie L, Zhu L T, Luo Z H, Jiang C W. Multiscale modeling of mixing behavior in a 3D atom transfer radical copolymerization stirred-tank reactor. Macromolecular Reaction Engineering 2017; **11**(2): 1600022.

22. Gallifuoco A. A new approach to kinetic modeling of biomass hydrothermal carbonization. ACS Sustainable Chemistry & Engineering 2019; **7**(15): 13073-13080.

23. Lucian M, Volpe M, Fiori L. Hydrothermal carbonization kinetics of lignocellulosic agro-wastes: experimental data and modeling. Energies 2019; **12**(3): 516.

24. Álvarez-Murillo A, Sabio E, Ledesma B, Román S, González-García C. Generation of biofuel from hydrothermal carbonization of cellulose. Kinetics modelling. Energy 2016; **94**: 600-608.

25. Reza M T, Yan W, Uddin M H, Lynam J G, Hoekman S K, et al. Reaction kinetics of hydrothermal carbonization of loblolly pine. Bioresource technology 2013; **139**: 161-169.

26. Keiller B G, Muhlack R, Burton R A, van Eyk P J. Biochemical Compositional Analysis and Kinetic Modeling of Hydrothermal Carbonization of Australian Saltbush. Energy & Fuels 2019.

27. Pecha M B, Arbelaez J I M, Garcia-Perez M, Chejne F, Ciesielski P N. Progress in understanding the four dominant intra-particle phenomena of lignocellulose pyrolysis: chemical reactions, heat transfer, mass transfer, and phase change. Green chemistry 2019; **21**(11): 2868-2898.

28. Funke A, Ziegler F. Heat of reaction measurements for hydrothermal carbonization of biomass. Bioresource technology 2011; **102**(16): 7595-7598.

29. Osoyo A, Elms R. United States Department of Agriculture Foreign Agricultural Service (USDA-MX2020-0049). 2020 [cited 2020 25/10]; Available from: https://www.fas.usda.gov/data/mexico-avocado-annual-5.

30. McLeod L, Flores D. USDA-Foreing-Agricultural-Service (2017) Mexico Avocado Annual. 2017 [cited 2020 25/10]; Available from: https://www.fas.usda.gov/data/mexico-avocado-annual-2.

31. Ceballos A M, Montoya S. Evaluación química de la fibra en semilla, pulpa y cáscara de tres variedades de aguacate. Biotecnología en el sector agropecuario y agroindustrial 2013; **11**(1): 103-112.

32. Perea-Moreno A-J, Aguilera-Ureña M-J, Manzano-Agugliaro F. Fuel properties of avocado stone. Fuel 2016; **186**: 358-364.

33. Mason P, Darvell L, Jones J, Williams A. Comparative study of the thermal conductivity of solid biomass fuels. Energy & Fuels 2016; **30**(3): 2158-2163.

34. Blackman C F, Black J A. Measurement of microwave radiation absorbed by biological systems: 2. Analysis by Dewar-flask calorimetry. Radio Science 1977; **12**(6S): 9-14.

35. Gyurik L, Egedy A, Zou J, Miskolczi N, Ulbert Z, et al. Hydrodynamic modelling of a two-stage biomass gasification reactor. Journal of the Energy Institute 2019; **92**(3): 403-412.

36. Almohammadi K, Ingham D, Ma L, Pourkashan M. Computational fluid dynamics (CFD) mesh independency techniques for a straight blade vertical axis wind turbine. Energy 2013; **58**: 483-493.

37. Jaszczur M, Młynarczykowska A, Demurtas L. Effect of Impeller Design on Power Characteristics and Newtonian Fluids Mixing Efficiency in a Mechanically Agitated Vessel at Low Reynolds Numbers. Energies 2020; **13**(3): 640.

38. Cullen P J, Food mixing: Principles and applications, in Book Food mixing: Principles and applications. 2009, John Wiley & Sons.

39. Mardles E. Viscosity of suspensions and the Einstein equation. Nature 1940; **145**(3686): 970-970.

40. Laskowski J, Surface chemistry fundamentals in fine coal processing, in The Coal Handbook: Towards Cleaner Production. 2013, Elsevier. p. 347-421.

41. Khaled C, Driss N, Nouredine S C. CFD simulation of turbulent flow and heat transfer over rough surfaces. Energy Procedia 2015; **74**: 909-918.

42. Frei W. Which turbulence model should I choose for my CFD application. Consulted on 2013; **7**(05): 2015.

43. Pecha M B, Ramirez E, Wiggins G M, Carpenter D, Kappes B, et al. Integrated Particle-and Reactor-Scale Simulation of Pine Pyrolysis in a Fluidized Bed. Energy & fuels 2018; **32**(10): 10683-10694.

44. Xue Q, Fox R O. Computational modeling of biomass thermochemical conversion in fluidized beds: particle density variation and size distribution. Industrial & Engineering Chemistry Research 2015; **54**(16): 4084-4094.

45. Dupont C, Chiriac R, Gauthier G, Toche F. Heat capacity measurements of various biomass types and pyrolysis residues. Fuel 2014; **115**: 644-651.

46. Gupta M, Yang J, Roy C. Specific heat and thermal conductivity of softwood bark and softwood char particles☆. Fuel 2003; **82**(8): 919-927.

47. Raznjevic K. Handbook of thermodynamic tables and charts. 1976.

48. Ragland K, Aerts D, Baker A. Properties of wood for combustion analysis. Bioresource technology 1991; **37**(2): 161-168.

49. Milosavljevic I, Oja V, Suuberg E M. Thermal effects in cellulose pyrolysis: relationship to char formation processes. Industrial & Engineering Chemistry Research 1996; **35**(3): 653-662.

50. Özcan-Taskin G, Wei H. The effect of impeller-to-tank diameter ratio on draw down of solids. Chemical engineering science 2003; **58**(10): 2011-2022.

51. Liu Z, Quek A, Hoekman S K, Balasubramanian R. Production of solid biochar fuel from waste biomass by hydrothermal carbonization. Fuel 2013; **103**: 943-949.

52. Merzari F, Lucian M, Volpe M, Andreottola G, Fiori L. Hydrothermal carbonization of biomass: design of a bench-Scale reactor for evaluating the heat of reaction. Chemical Engineering Transactions 2018; **65**: 43-48.

Graphic abstract

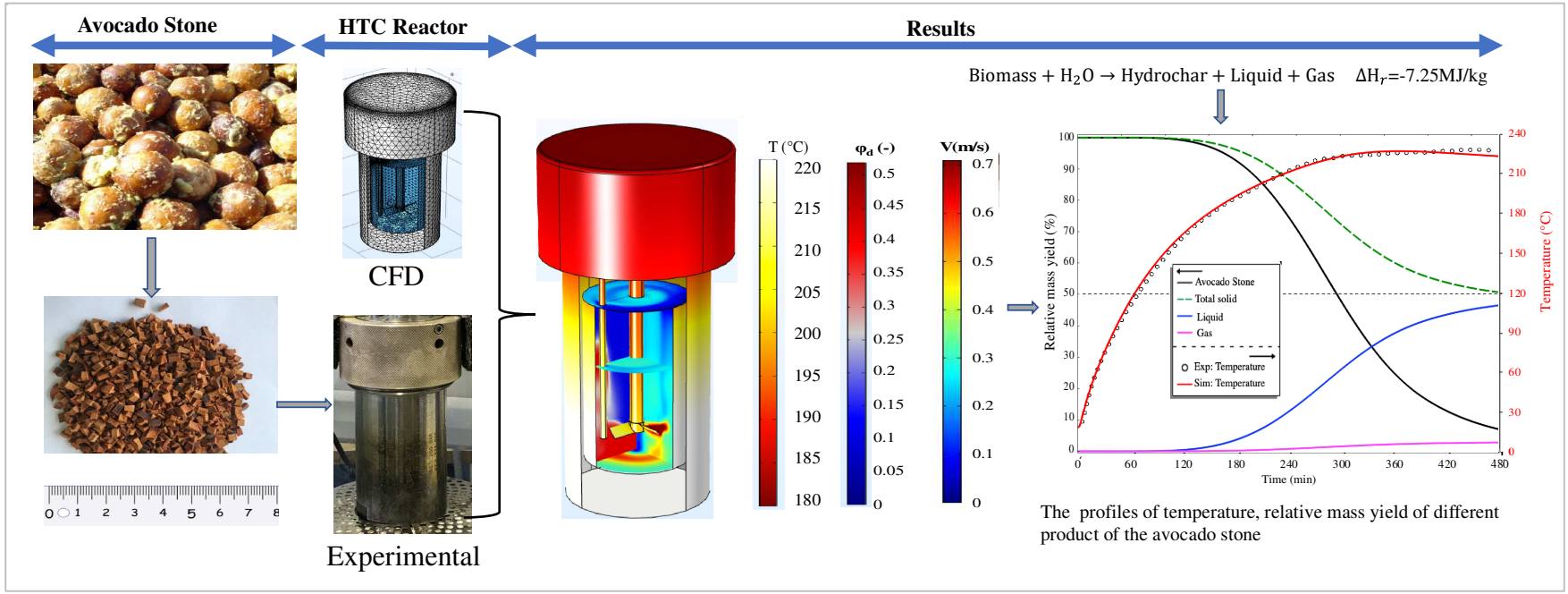

The profiles of temperature, relative mass yield of different product of the avocado stone